Journal of Solid State Electrochemistry
https://doi.org/10.1007/s10008-023-05593-9

ORIGINAL PAPER

Localized corrosion of 15–5 PH and 17–4 PH stainless steel in NaCl solution

Brisa Martínez-Aparicio[1] · David Martínez-Bastidas[2] · Citlalli Gaona-Tiburcio[1] · Ulises Martin[2] · José Cabral-Miramontes[1] · Facundo Almeraya-Calderón[1]

Received: 2 January 2023 / Revised: 26 June 2023 / Accepted: 6 July 2023

Abstract
The importance in the selection of materials in the aeronautical industry for the manufacture of an aircraft is related to the fact that the materials are present during the life cycle of the aircraft. In particular, the precipitation hardening (PH) stainless steel is used in components that require the combination of excellent mechanical properties, as well as corrosion resistance due to aircraft exposure in harsh environments. Inherently corrosion resistant steels achieve an important characteristic which is passivation by forming a protective layer of chromium oxide on the surface. This research aimed to conduct an analysis of the localized corrosion on stainless steel 15–5 PH and 17–4 PH, used on fasteners or engine components. The steels were evaluated in a 3.5 wt.% NaCl solution, using the electrochemical technique of cyclic potentiodynamic polarization curves (CPP) according to the ASTM 61–86 standard. The microstructural analysis was performed by optical microscopy (OM) and scanning electron microscopy (SEM). The results indicated that CPP curves showed a positive hysteresis, indicating pitting localized corrosion and the corrosion current density of the 15–5 PH and 17–4 PH stainless steels were 1.31×10^{-8} and 2.70×10^{-8} A/cm^2.

Keywords Stainless steel · Pitting corrosion · Cyclic potentiodynamic polarization · Passivity breakdown

Introduction

The corrosive attack of materials in the aeronautical industry accounts for approximately 31% of the failure modes in an aircraft, affecting economic, safety, and logistic issues [1]. Stainless steels are widely used in the industry due to their excellent mechanical resistance, corrosion resistance, and impact resistance [2, 3]. The use of steel in an aircraft is limited, as not all grades of steel can be used and only a small group has the high strength and toughness required in aircraft structures. Precipitation hardening stainless steel is one of the major categories with aeronautical applications due to its unique combination of high mechanical properties and corrosion resistance. This alloy, known for its exceptional properties and characteristics, is extensively utilized across numerous vital parts and components within aircraft structures and engines. Its widespread application can be attributed to its superior strength, durability, and resistance to high temperatures and corrosive environments [4–6]. Stainless steel categories are determined by their microstructure and composition, which include austenitic, martensitic, ferritic, and duplex. However, for the precipitation hardening stainless steels, their classification is determined mostly by the method of heat treatment used rather than their microstructure alone [7]. In precipitation hardenable stainless steels, their chemical composition includes aluminum, copper, and titanium as alloying elements that contribute to solution hardening and heat treatment for aging. Also, this type of steel has a subclassification into martensitic, semi-austenitic, and austenitic. As for aircraft precipitation hardening stainless steels, they are those with a high-strength martensitic tempered microstructure and a surface layer of chromium oxide that protects against corrosion [3].

Martensitic grades have higher carbon (C) content compared to other grades to improve strength and hardenability; sometimes nitrogen (N) is added to further improve strength. Other elements present in the chemical composition are

✉ Brisa Martínez-Aparicio
brisa.martinezpr@uanl.edu.mx

[1] FIME–Centro de Investigación e Innovación en Ingeniería Aeronáutica CIIA, Universidad Autónoma de Nuevo León, Nuevo León, Mexico

[2] National Center for Education and Research On Corrosion and Materials Performance, Dept. Chemical, Biomolecular, and Corrosion Engineering, NCERCAMP-UA, The University of Akron, Akron, OH, USA

Published online: 25 July 2023

small amounts of nickel (Ni) and molybdenum (Mo) and to improve machinability.sulfur (S) is occasionally added.

The addition of elements such as Ni and reducing the C content can improve the weldability of the martensitic grade of stainless steel, as it is not a very good property in this type of steel. The martensitic grade has the characteristic of being magnetic and hardenable. Hence, the property of being hardenable allows the obtaining of precipitation-hardening stainless steel grades, which is achieved through a special mechanism that involves the formation of precipitates inside the microstructure [8].

One of the highly regarded stainless steel grades in the aeronautical sector for its precipitation hardening capabilities is 17–4 PH. This grade is characterized by its low carbon content, not exceeding 0.07%, and significant amounts of chromium ranging from 15 to 17.5%. Additionally, it incorporates nickel in the composition, typically ranging from 3 to 5%, along with other essential alloying elements [7, 8]. Similarly, there is 15–5 PH stainless steel also for aeronautical applications, designed to improve toughness compared to 17–4 PH stainless steel. The distinctive feature of stainless steels is undoubtedly their resistance to corrosion. Nevertheless, these stainless-steel grades are not immune to various types of corrosion. Factors such as insufficient preventive treatments, environmental conditions, application, and others can contribute to corrosion occurrence. Corrosion poses a significant challenge within the aeronautical industry, prompting a compelling need to study and address this issue. The study of corrosion in this context is driven by three fundamental reasons: ensuring safety, optimizing economic considerations, and preserving the longevity and performance of aircraft. Regarding the study of corrosion resistance in stainless steels, different authors have conducted extensive research and investigations. These studies aim to deepen our understanding of the factors influencing corrosion behavior, identify potential corrosion mechanisms, and evaluate the performance of different stainless-steel compositions in various environments. For example, Lara et al. [9] conducted a study involving a passivation treatment on samples of 15–5 PH and 17–4 PH stainless steels. The researchers observed that the passivated samples exhibited a notable improvement in corrosion resistance compared to the non-passivated ones. This improvement was evidenced by a decrease in the corrosion rate, as indicated by the potentiostatic polarization curves (PPC). In the study conducted by Ameer et al. [10], it was observed that the corrosion current (i_{corr}) values of stainless steel increased as the concentration of $Cl-$ or $SO_4{}^{2}-$ ions increased. The findings indicate a decrease in the formation of the passive film on the surface of the stainless steel and this was determined through potentiodynamic polarization (PP) testing. Adbo et al. [11] evaluated the formation of pitting in a laser-welded 2205 duplex stainless steel in a seawater environment (3.5 wt.% NaCl) through EIS and PPC techniques. Marcelin et al. [12] analyzes the electrochemical behavior of martensitic stainless steels in different experimental conditions, where it was found that in the passive state, the corrosion process was controlled by the properties of the passive film during air exposure. Bragaglia et al. [13] used PP to observe the behavior of passivated and non-passivated 304 austenitic stainless steels in acid electrolytes. The pitting potential in nitric acid increases when the steel is passivated. In a comparative study conducted by Martínez et al. [14], the corrosion behavior of passivated 15–5 PH stainless steel (SS) samples, treated with citric acid, was assessed using the CPP technique. The results revealed that the passivated samples exhibited only minor increases in current, indicating the preservation of the protective passive layer on the surface. However, the blank sample (without passivation) displayed significant current increments, leading to the breakdown of the passive layer and the formation of localized corrosion pits. Recently, there has been a growing interest in conducting investigations into various aspects of precipitation hardening stainless steels, focused on fatigue behavior, hydrogen diffusion, and microstructural characterization [15–17]. Gaona et al. [18] studied the corrosion behavior of AM350 passivated PHSS steels using electrochemical noise, potentiodynamic polarization, and electrochemical impedance spectroscopy in acid baths. Abad et al. [19] study conducted to simulate the effects of stray current and salt water environmental conditions of 15-5PH H1025 stainless steel, which is a common material used on aircraft. It was determined that with time, the condition of 71 °C tap water with current formed corrosion pits on this material.

The martensitic precipitation hardening stainless steels showed the best results for corrosion behavior in acid solutions. Other authors as Samaniego et al. [20] studied that passivation in nitric acid baths made the surface prone to the localized corrosion process. Almeraya et al. [21] analyzed the passivate state of martensitic PHSS passivated in citric and nitric acid, where nitric acid presented the lowest corrosion values.

Over the past few years, the corrosion behavior of austenitic stainless steels has been extensively studied. Passivated PHSS have had few studies, so it is important to know the behavior of electrochemical corrosion in environments that simulate aircraft working conditions, such as marine and industrial atmospheres.

The aim of this work is to investigate the localized corrosion behavior of 15-5PH and 17-4PH precipitation hardening stainless steels through electrochemical testing using cyclic potentiodynamic polarization (CPP) in a 3.5 wt.% NaCl solution. The corrosion phenomena will be further analyzed through microscopic characterization techniques, including optical microscopy (OM) and scanning electron microscopy (SEM). These stainless-steel alloys are widely utilized in the aeronautics industry and are subjected to

Table 1 Chemical composition of 15-5PH and 17–4 PH stainless steel (wt.%)

Stainless steel	C	Mn	Si	Cr	Ni	N	Cu	Mo	Co	Fe
15–5 PH	0.07	0.88	0.54	13.8	4.37	0.50	3.13	0.34	0.23	Balance
17–4 PH	0.07	0.76	0.49	14.8	4.36	-	3.10	0.21	-	Balance

diverse environmental conditions, including marine and industrial atmospheres, which may include corrosive elements such as chlorides and acid rain, respectively.

Experimental procedure

Elemental composition and microstructure

The employed stainless steels were commercial precipitation hardening stainless steels (AMS Aerospace Material Specifications) 15-5PH (AMS 5659) and 17-4PH (AMS 5643) obtained in cylindrical extruded bar with a diameter of 0.5 in and a length of 10 in. The chemical composition of the 15–5 PH and 17–4 PH was determined by atomic absorption spectrometry (AAS); the results are shown in Table 1.

The microstructures of the 15–5 PH and 17–4 PH alloys were obtained through optical microscopy shown in Fig. 1. In the microstructures, a mostly laminar tempered martensitic (α′) phase matrix is observed, characteristic of this type of steel, as well as the presence of elongated islands of austenite (γ) phase at the grain boundaries. Stainless steel samples were prepared according to ASTM E3-11 standard [22]. From the cylindrical steel rod, coupons of approximately 3/8″ × ½” thickness were obtained, and the samples were mechanically polished using different SiC papers (400, 500, 600, and 800 grade). Subsequently, the samples were subjected to ultrasonic cleaning according to the ASTM A380-17 standard [23]. The polished sample etching was to reveal the microstructure of steel, followed by 10 min of ultrasonic cleaning in deionized water.

Electrochemical testing

Corrosion experiments were conducted to investigate the corrosion behavior of the stainless-steel samples (15–5 PH and 17–4 PH). The experiments involved immersing the samples in a 3.5 wt.% sodium chloride (NaCl) solution at room temperature using a Gill AC equipment (potentiostat/galvanostat). To ensure accurate and reliable results, the stainless-steel samples were carefully prepared and had an exposed surface area of 1.0 cm^2.

The choice of a 3.5 wt.% NaCl solution for the corrosion experiments is significant. This solution represents a simulated marine environment and is commonly used as a standard corrosive medium to assess the corrosion resistance of materials [24]. By subjecting the stainless-steel samples to this solution, the experiments aimed to simulate the corrosive conditions encountered in marine environments, which are known for their potential to induce localized corrosion and pitting.

A typical corrosion cell was composed of three electrodes, a working electrode (WE), which is the stainless-steel sample (15–5 PH or 17–4 PH), a reference electrode (RE, saturated calomel (SCE)), and a counter electrode (CE) a platinum mesh. Initially, electrochemical corrosion potential (E_{corr}) was supervised until a steady state value was reached. CPP tests were performed according to ASTM 61–86 standard [25] to obtain information related to the dissolution reaction kinetics of the electrochemical corrosion. CPP curves were recorded using a polarization scan from − 1 V to + 1.2 V vs E_{corr}, with a scan rate of 1 mV/s.

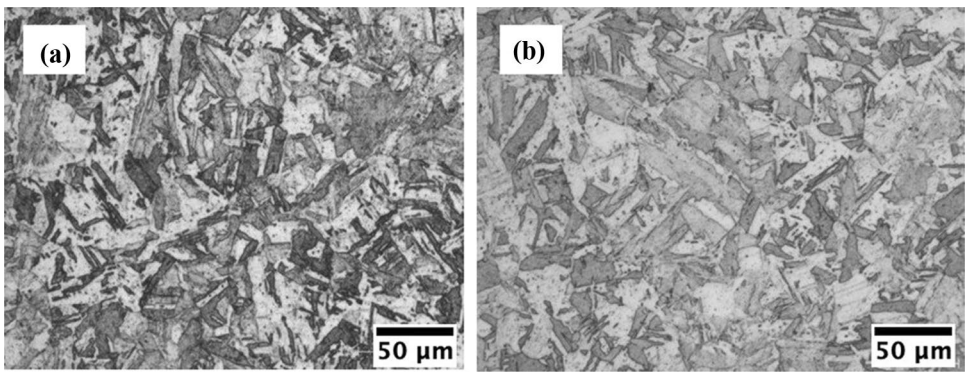

Fig. 1 OM microstructure of stainless-steel samples: **a** 15–5 PH and **b** 17–4 PH

Microstructural characterization

Optical microscopy (OM, Olympus, Hamburg, Germany) was used to determine the microstructure of 15–5 PH or 17–4 PH. The use of SEM (Hitachi 3030 equipment) contributed to the punctual study of corrosion products using a backscattered electron (BSE) detector at × 30 and × 200 magnifications for the sample of 15–5 PH, and for the sample of 17–4 the magnifications were × 30 and × 300. Also, with an X-ray energy dispersive spectroscopy (EDS) detector, it was possible to recognize elements of interest in the samples.

Results and discussion

Resistance to pitting corrosion

In stainless steel, the carbon content decreases corrosion resistance. Still, it increases toughness and causes greater susceptibility to formation chromium carbides that can embrittle the material due to precipitation at grain boundaries.

Resistance to pitting corrosion can be measured using the pitting resistance equivalent number (PREN). This parameter is based on the chemical composition of stainless steels, and the PREN result indicated greater resistance to pitting corrosion at high values [26, 27], see Table 2. It is calculated (Eq. (1)) based on the chromium (Cr), molybdenum (Mo), tungsten (W), and nitrogen (N) content of an alloy [28]. In this sense, of the stainless steels evaluated in this work, the 15-5PH and 17-4PH alloys, were the ones that presented the highest PREN value with 22.9 and 15.4, respectively. Therefore, based on these results, 15-5PH should present greater resistance to pitting corrosion (see Table 2).

$$PREN = Cr + 3.3Mo + 16N \quad (1)$$

Electrochemical measurements

The corrosion kinetic behavior using potentiodynamic polarization can be observed through cathodic and anodic reactions in polarization curves to obtain the electrochemical parameters (corrosion current density, i_{corr} (μA·cm^2), potential corrosion, E_{corr} (mV), and corrosion rate).

Table 2 Pitting resistance equivalent numbers of the precipitation hardening stainless steel

PHSS	Cr	Mo	N	PREN
15-5PH	13.8	0.34	*0.50*	*22.9*
17-4PH	14.8	0.21	–	15.4

The application of the CPP technique allowed obtaining measurements for the determination of the initiation and propagation of localized corrosion (pitting) in precipitation hardening stainless steel. Similarly, it was possible to identify the passivation zone, breakdown of the passive layer, and measure current densities to process the values and obtain the corrosion rate [25]. The CPP results presented in Fig. 2a, b show the electrochemical behavior of the sample of stainless steels 15–5 PH and 17–4 PH in a 3.5 wt.% NaCl electrolyte solution.

Figure 2a shows the results for CPP curve of 15–5 PH stainless steel sample where an initial activation process is observed and then the passivity plateau (ΔE_{pass}) is revealed from − 0.20 to 0.14 V. Additionally, small variations in the current are observed due to increases in it that correspond to metastable pitting registered at current densities close to 10^{-7} A/cm^2, which finally generated a passive film breakdown causing pitting. Current densities in the passivity plateau (i_{pass}) values recorded were in the order of 6.67×10^{-7} A/cm^2 [14, 18, 19] and corrosion current density values were in the order of 1.31×10^{-8} A/cm^2.

In the same way, Fig. 2b corresponds to the electrochemical behavior of 17–4 PH stainless steel evaluated in 3.5 wt.% NaCl electrolyte solution. Initially, a positive hysteresis attributable to pitting can be observed. Recorded i_{pass} current densities presented values in the order of 1.35×10^{-6} A/cm^2 [14], and for the corrosion current density values were in the order of 2.70×10^{-8} A/cm^2. A large passivity plateau was observed for 15–5 PH than 17–4 PH stainless steel, 183.7 and 155.2 mV, respectively.

The backward CPP scan displayed no repassivation of the samples, as it can be shown by the backward scan intersection with the active dissolution branch of the forward CPP scan. In addition, the stable pitting is also indicated by the large hysteresis loop found before the potential scan was swapped to cathodic potential direction.

In general, the CPP for the stainless-steel samples of 15–5 PH and 17–4 PH evaluated in 3.5 wt.% NaCl represents the corrosion potential vs. the logarithm of the current, indicating a mixed control by activation which, in turn, reveals the behavior of the corrosion kinetics. The parameters obtained from cyclic potentiodynamic polarization are summarized in Table 3.

Pitting potential (E_{pit}) is the potential value at which the current increases and the pitting attack occurs [15]. The 15–5 PH and 17–4 PH stainless steel samples had pitting potential values of 149.3 mV and 149.8 mV, respectively, then an increase occurs in the corrosive density in the transpassivation stage.

The shapes of the potentiodynamic polarization curves (Fig. 2a and b) of the PHSS steels are similar; the anodic reaction begins in activation, followed by a passivation, with similar pitting potential and positive hysteresis.

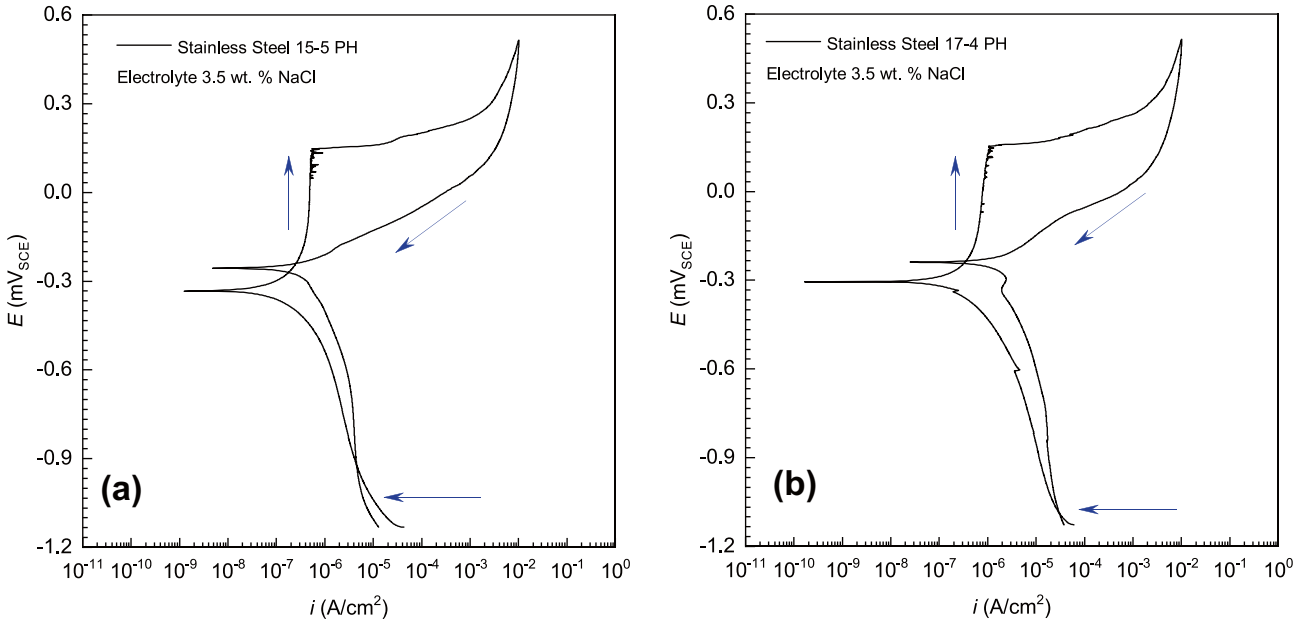

Fig. 2 Cyclic potentiodynamic polarization curves, scan rate of 1 mV/s **a** 15–5 PH stainless steel, and **b** 17–4 PH stainless steel, immersed in 3.5 wt.% NaCl solution

The passivation protection mechanism occurs when the passivation film formed on the surface of the Cr–Fe alloy determined its corrosion resistance. Chromium oxides play an important role in passive films and the behavior is attributed to the anodic reactions of the OH −. The increase in the current density in the PHSS samples gives rise to the transpassivation [29–33].

According to some authors [34–37], the results indicated that during passivation in the PHSS, there is a relatively stable range of passive potential. The passive current density is the same, which indicates that it forms a relatively stable passive film. However, if the electrochemical process is still active in the anodic reaction, the passive current density is not the same, and the passive film is unstable.

SEM surface characterization

Surface characterization was conducted using Scanning Electron Microscopy (SEM) using a backscattered electron (BSE) imaging; the morphology of the surface of the PH stainless steel samples evaluated in the 3.5 wt.% NaCl electrolyte solution was determined. Using EDS technique, the semiquantitative elemental composition (elements present in the analysis areas) was obtained. Figure 3 shows the morphology of the surface by SEM-BSE of the 15–5 PH stainless steel corresponding to × 30 and × 200 magnifications, as detailed, respectively. The samples have a considerable density of pits with sizes of 1 mm in some cases. In addition, Fig. 4a shows the morphology of some pitting caused by the sodium chloride solution; the pitting has a size of 50 to 100 µm.

In addition, Fig. 4a shows the morphology of some pitting caused by the sodium chloride solution; the pitting has a size of 50 to 100 µm. In the EDS spectrum depicted in Fig. 4b, elemental analysis revealed the presence of iron, chromium, and manganese, which are part of the 15–5 PH stainless steel alloy, in addition to sodium and chlorine from the NaCl solution tested.

In the same way, Fig. 5 presents the mapping of elements by EDS, where it is observed that Na and Cl are in the entire periphery surrounding the pits and the other elements are distributed throughout the alloy.

The results in Fig. 6 show the morphology of the surface by SEM -BSE of 17–4 PH stainless steel at different magnifications, × 30 and × 300. The 17–4 PH sample presents a

Table 3 Electrochemical parameters obtained by CPP test by 15-5PH and 17–4 PH stainless steel exposed in NaCl solutions

Stainless steel	E_{corr} (mV)	E_{pit} (mV)	$\lvert\Delta E_{pass}\rvert$ (mV)	i_{pass} (A/cm^2)	i_{corr} (A/cm^2)	*Hysteresis*
15–5 PH	− 335	149.3	183.7	6.67×10^{-7}	1.31×10^{-8}	Positive
17–4 PH	− 305	149.8	155.2	1.35×10^{-6}	2.70×10^{-8}	Positive

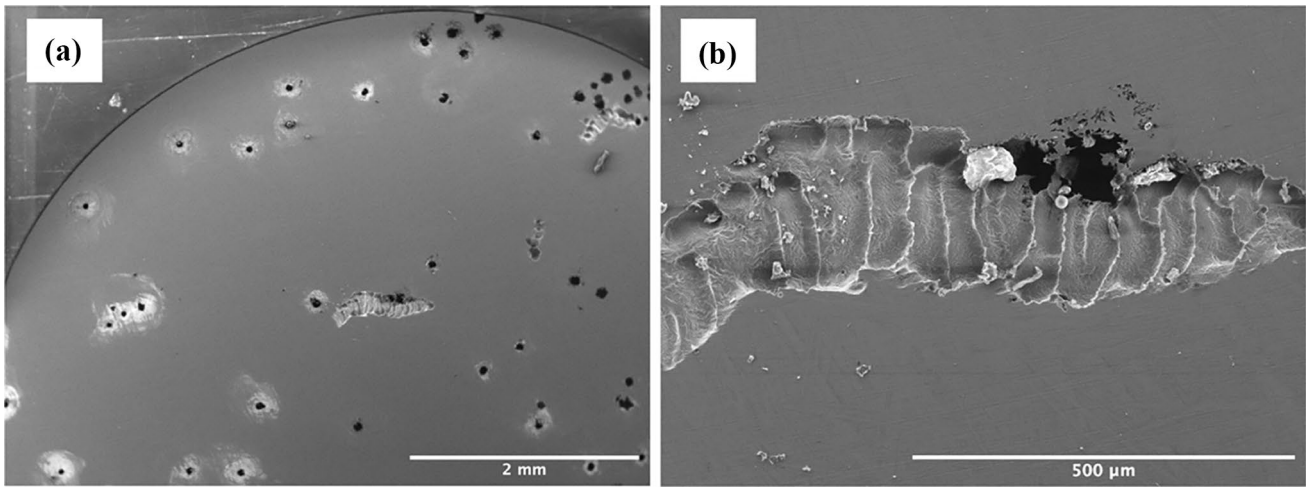

Fig. 3 SEM-BSE surface morphology obtained of 15–5 PH stainless steel sample after CPP test in 3.5 wt.% NaCl electrolyte solution: **a** × 30 and **b** × 200 magnifications

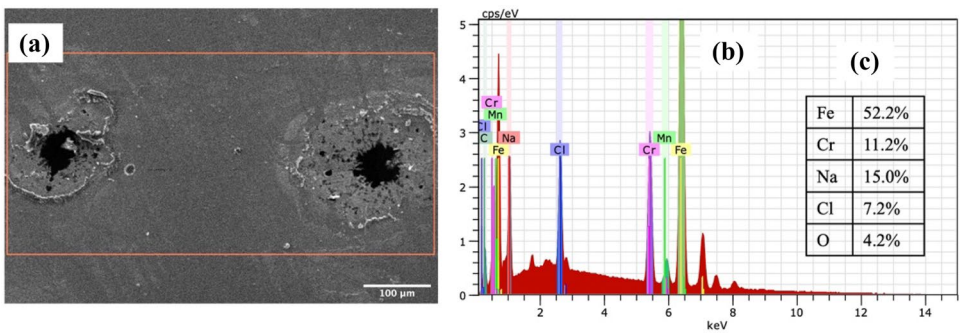

Fig. 4 SEM-BSE 15–5 PH stainless steel sample: **a** surface morphology, × 30; **b** EDS spectrum, and **c** elemental analysis percentages

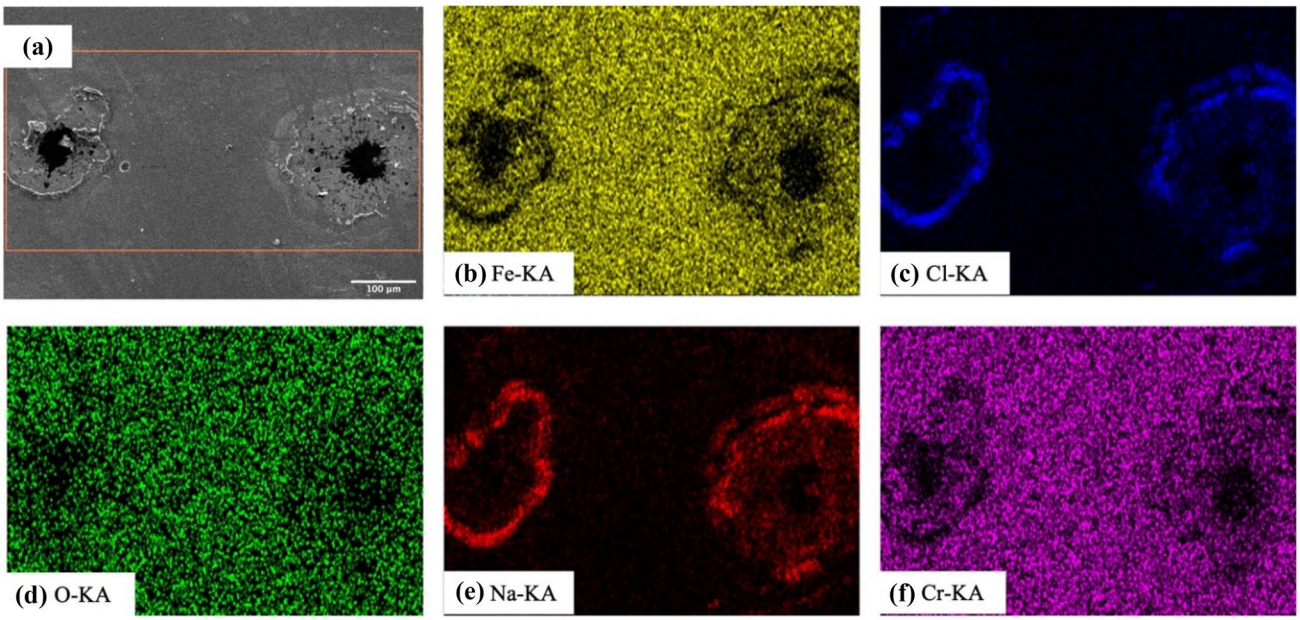

Fig. 5 SEM–EDS elemental mapping in the area of interest of 15–5 PH stainless steel, **a** surface morphology, **b** Fe, **c** Cl, **d** O, **e** Na, and **f** Cr

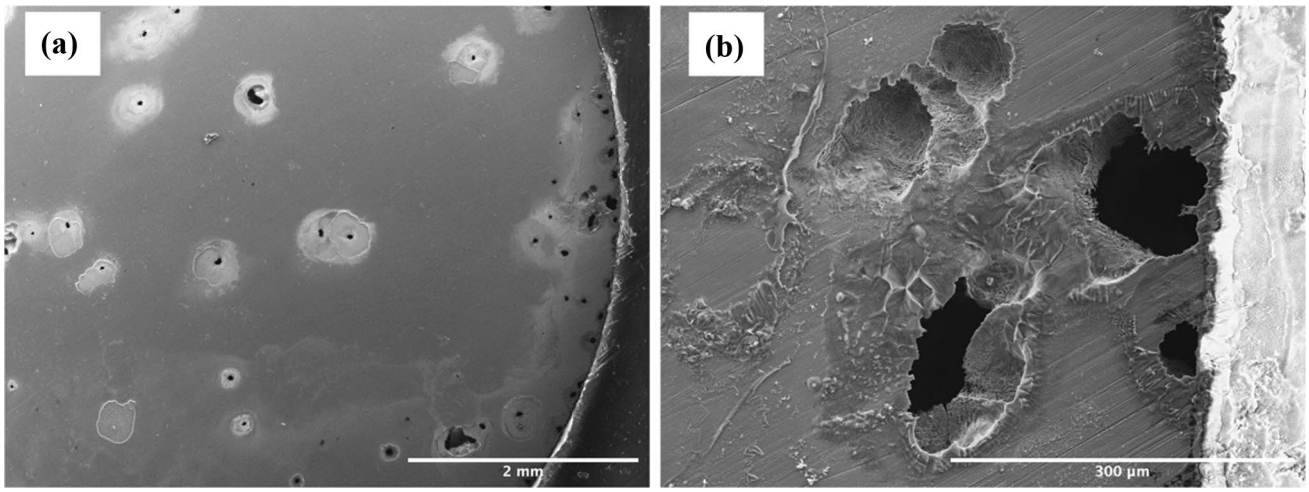

Fig. 6 SEM-BSE surface morphology of the 17–4 PH stainless steel sample after CPP test in 3.5 wt.% NaCl solution, **a** × 30 and **b** × 300 magnifications

higher pit density compared to the 15-5PH sample as well as wider and deeper pits [38].

The surface morphology of the pits revealed on the stainless steel 17–4 PH has a size of 20 µm (Fig. 7a); in addition chloride attack was preferentially found on the edges of the pit, causing the pits to nucleate on the surface of the stainless steel. In the EDS spectrum (Fig. 7b), the distinctive elements of the alloy are observed, such as iron and chromium, also the presence of sodium and chlorine and some traces of oxygen, respectively.

In the elemental EDS mapping shown in Fig. 8, sodium and chlorine are found surrounding the entire contour of the pits, as well as the pit mount, while other elements (Fe, Cr, O) are homogeneously distributed throughout the alloy. According to the literature [39, 40], the passive protective film formed on stainless steel surfaces is highly attributed to the corrosion resistance in these steels. The double-layer structure of SS passive film has a double-layer structure that is rich in Fe and Cr, respectively. Chromium oxides play a significant role in the corrosion resistance of PHSS. Cr3 + has higher anticorrosion stability compared to FeO and Fe2O3 oxides. Therefore, the Cr2O3 content in the stainless-steel passive film is a primary factor for the stability and anticorrosive property of the steel. Defects will form in the passive film, leading to the nucleation of localized corrosion (generating pitting). On the other hand, the defect density of the iron-rich outer layer is higher than that of the chromium-rich inner layer, which could lead to the absorption of a large amount of Cl^- in the passive film in PHSS.

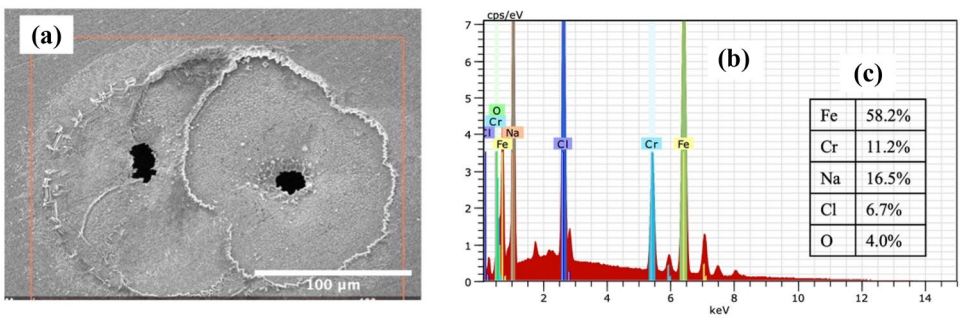

Fig. 7 SEM-BSE surface morphology, **a** 17–4 PH stainless steel sample, **b** EDS spectrum, and **c** elemental analysis percentages

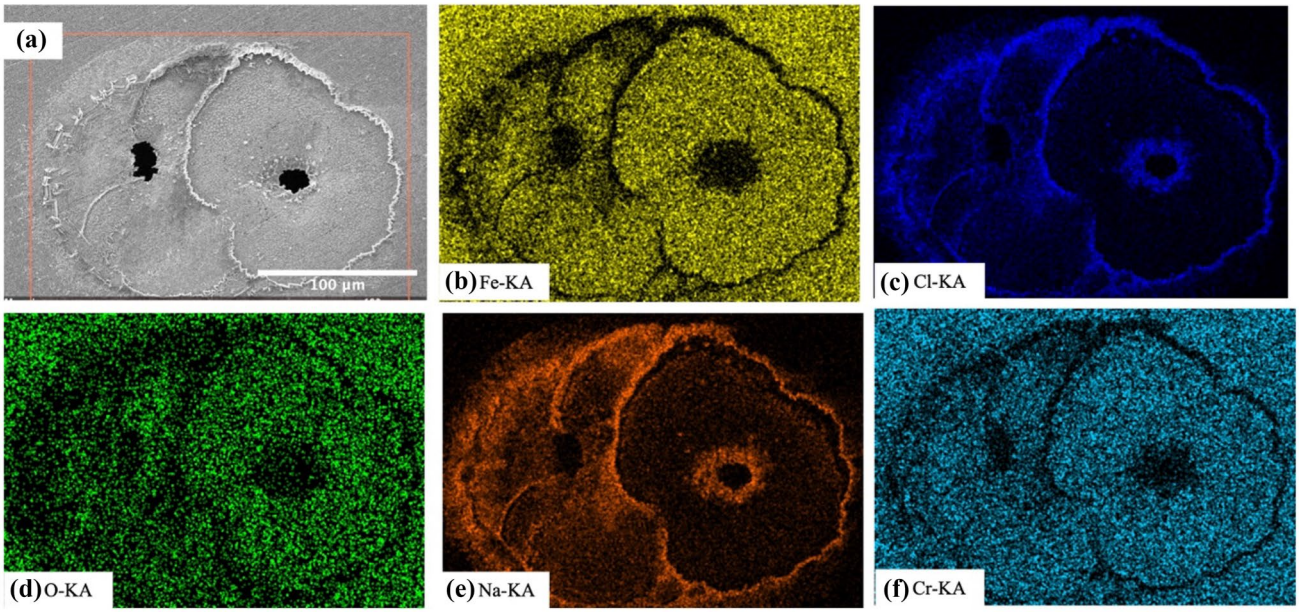

Fig. 8 SEM–EDS elemental mapping in the area of interest of 17–4 PH stainless steel, **a** surface morphology, **b** Fe, **c** Cl, **d** O, **e** Na, and **f** Cr

Conclusions

This research focused on investigating the localized corrosion behavior of 15-5PH and 17-4PH stainless steels. Through a comprehensive analysis of the experimental findings, the following conclusions can be drawn:

1. The electrochemical assessment of the PHSS samples using cyclic potentiodynamic polarization (CPP) curves revealed the presence of a positive hysteresis. This phenomenon indicates the occurrence of localized corrosion in the form of pitting when the samples were tested in a 3.5 wt.% NaCl solution.
2. Likewise, fluctuations generated by small current increments corresponding to metastable pitting were observed in the samples (15-5PH and 17-4PH) which favors the passive film breakdown and the initiation of pits. Regarding the corrosion current density value was 1.31×10^{-8} A/cm2 for 15-5PH and 2.70×10^{-8} A/cm2 corresponds to 17-4PH. Moreover, localized corrosion (pitting) can be observed and corroborated by SEM, where a higher density of pits is found for the 17–4 PH as compared to the 15–5 PH stainless steel, showing a 50 and 20 µm pit size, respectively, attributed to the percentage of molybdenum in the composition of the alloys.
3. OM characterization indicated that 15–5 PH and 17–4 PH alloys shown a martensitic (α′) phase as well as the presence of elongated islands of austenite (γ) phase at the grain boundaries, respectively.
4. The resistance to pitting corrosion was determined by calculating the pitting resistance equivalent number (PREN). Among the stainless steel alloys investigated, it was observed that 15-5PH exhibited the highest PREN value of 22.9. This indicates that SS 15-5PH has a greater ability to resist pitting corrosion compared to the SS 17–4 PH.

Acknowledgements The authors appreciate the Autonomous University of Nuevo León and the University of Akron for the facilities granted to carry out this research, as well as the CONACYT Basic Science Project No. A1-S-8882. The authors acknowledge the technical support and facilities from The National Center for Education and Research on Corrosion and Materials Performance (NCERCAMP-UA), The College of Engineering and Polymer Science, and The University of Akron.

Funding The authors gratefully acknowledge the financial support from Firestone Research Grant 639430, and The University of Akron Fellowship programs FRC-207160 and FRC-207865.

References

1. Findlay SJ, Harrison ND (2002) Why aircraft fail. Mater Today 5:18–25. https://doi.org/10.1016/S1369-7021(02)01138-0
2. Mouritz PA (2012) Introduction to aerospace materials, 1st edn. Woodhead Publishing Limited, Cambridge, United Kingdom
3. Gialanella S, Malandruccolo A (2020) Aerospace alloys, 1st edn. Springer Nature, Switzerland
4. Eswara Prasad RWN (2009) Aerospace materials and technologies - Vol 1 Aerospace materials. Springer Science + Business Media, Singapore

5. Beddoes J, Parr JG (1999) Introduction to stainless steels, Ed. ASM International
6. Gloria A, Montanari R, Richetta M, Varone A (2019) Metals 9:662. https://doi.org/10.3390/met9060662
7. Farrar J (2004) The alloy tree—a guide to low-alloy steels, stainless steels and nickel-base alloys. Woodhead Publishing Limited and CRC Press, Sawston, UK
8. Outokumpu, (2013) High performance stainless steel. Handbook of Stainless Steel, Sweden
9. Lara-Banda M, Gaona-Tiburcio C, Zambrano-Robledo P, Delgado EM, Cabral-Miramontes JA, Nieves-Mendoza D, Maldonado-Bandala E, Estupiñan-Lopez F, Chacón-Nava JG, Almeraya-Calderón F (2020) Materials 13:2836. https://doi.org/10.3390/ma13122836
10. Ameer MA, Fekry AM, El-TaibHeakal F (2004) Electrochim Acta 50:43–49. https://doi.org/10.1016/j.electacta.2004.07.011
11. Abdo HS, Seikh AH, Abdus Samad, U, Fouly A, Mohammed JA (2021) Crystals 11:1225. https://doi.org/10.3390/cryst11091025
12. Marcelin S, Pébère N, Régnier S (2013) Electrochim Acta 87:32–40. https://doi.org/10.1016/j.electacta.2012.09.011
13. Bragaglia M, Cherubini V, Cacciotti I, Rinaldi M, Mori S, Soltani P, Nanni F, Kaciulis S, Montesperelli G (2015) Citric acid aerospace stainless steel passivation: a green approach. In Proceedings of the CEAS Aerospace Europe Conference 2015, Delft, The Netherlands, 7–11 September
14. Martinez-Aparicio BS, Gaona-Tiburcio C, Bastidas DM, Lara-Banda M, Samaniego-Gámez O, Almeraya-Calderon F (2022) ECS Trans 106(1):223–228. https://doi.org/10.1149/10601.0223ecst
15. Mollapour Y, Poursaeidi E (2021) Experimental and numerical analysis of pitting corrosion in CUSTOM 450 stainless steel. Eng Fail Anal 128:105589. https://doi.org/10.1016/j.engfailanal.2021.105589
16. Lin CK, Chu CC (2000) Mean stress effects on low-cycle fatigue for a precipitation-hardening martensitic stainless steel in different tempers. Fatigue Fract Eng Mater Struct 23:545–553. https://doi.org/10.1046/j.1460-2695.2000.00324.x
17. Garcia-Cabezon C, Castro-Sastre MA, Fernandez-Abia AI et al (2022) Microstructure-hardness-corrosion performance of 17–4 precipitation hardening stainless steels processed by selective laser melting in comparison with commercial alloy. Met Mater Int 28:2652–2667. https://doi.org/10.1007/s12540-021-01155-8
18. Gaona Tiburcio C, Samaniego-Gámez O, Jáquez-Muñoz J, Baltazar-Zamora MA, Landa-Ruiz L, Lira-Martínez A, Flores-De los Rios JP, Cabral-Miramontes J, Estupinán-López F, Almeraya-Calderon F (2022) Frequency-time domain analysis of electrochemical noise of passivated AM350 stainless steel for aeronautical applications. Int J Electrochem Sci 17:220950. https://doi.org/10.20964/2022.09.49
19. Abad A, Hahn M, Es-Said OS (2010) Corrosion of 15–5PH H1025 stainless steel due to environmental conditions. Eng Fail Anal 17(1):208–212. https://doi.org/10.1016/j.engfailanal.2009.06.004
20. Samaniego-Gámez O, Almeraya-Calderón F, Chacón-Nava J, Maldonado-Bandala E, Nieves-Mendoza D, Flores-De Los Rios JP, Jáquez-Muñoz JM, Delgado AD, Gaona-Tiburcio C (2022) Metals 12:666. https://doi.org/10.3390/met12040666
21. Almeraya-Calderón F, Samaniego-Gámez O, Maldonado-Bandala E, Nieves-Mendoza D, Olguín-Coca J, Jáquez-Muñoz JM, Cabral-Miramontes J, Flores-De los Rios JP, Bautista-Margulis RG, Gaona-Tiburcio C (2022) Metals 12:1033. https://doi.org/10.3390/met12061033
22. ASTM E3–95 (1995) Standard practice for preparation of metallographic specimens. ASTM International: West Conshohocken, PA, USA
23. ASTM A380–17 (2017) Standard practice for cleaning descaling and passivation of stainless-steel parts, equipment and systemsASTM International, West Conshohocken, PA, USA. https://doi.org/10.1520/A0380_A0380M-17
24. ASTM G44–99 (2013) Standard practice for exposure of metals and alloys by alternate immersion in neutral 3.5 % sodium chloride solution. ASTM International, West Conshohocken, PA, USA
25. ASTM G61–86 (2018) Standard test method for conducting cyclic potentiodynamic polarization measurements for localized corrosion susceptibility of iron-nickel, or cobalt- based alloysASTM International, West Conshohocken, PA, USA. https://doi.org/10.1520/G0061-86R18
26. Ramirez-Arteaga AM, Gonzalez-Rodriguez JG, Campillo B, Gaona-Tiburcio C, Dominguez-Patiño G, Leduc Lezama L, Chacon-Nava JG, Neri-Flores MA, Martinez-Villafañe A (2010) Int J Electrochem Sci 5:1786–1798
27. The British Stainless Steel Association 2022. https://bssa.org.uk/bssa_articles/calculation-of-pren. Accessed on 2 June 2022.
28. Schweitzer P (2007) Fundamentals of metallic corrosion: atmospheric and media corrosion of metals. CRC Press Taylor & Francis Group: Boca Raton, FL, USA. ISBN 10:0-8493-8243-2
29. Olsson C-OA (2018) Wet corrosion of stainless steels and other chromium-bearing alloys. In Encyclopedia of interfacial chemistry; Surface Science and Electrochemistry; Elsevier: Bonn, Germany 535–542. https://doi.org/10.1016/B978-0-12-409547-2.13583-8
30. Bojinov M, Fabricius G, Laitinen T, Saario T (1998) J Electrochem Soc 145:2043–2050
31. Tian H, Sun F, Chu F, Wang L, Wang X, Cui Z (2021) J Electroanal Chem 886:115138
32. Zhu Z, Zhang Q, Liu P, Zhang J, Cao F (2020) J Electroanal Chem 871:114107
33. Duan Z, Man C, Dong C, Cui Z, Kong D, Wang L, Wang X (2020) Corros Sci 167:108520
34. Noh LS, Laycock NJ, Gao W, Wells DB (2000) Corros Sci 42:2069–2084. https://doi.org/10.1016/S0010-938X(00)00052-4
35. Choudhary S, Qiu Y, Thomas S, Birbilis N (2020) Electrochim Acta 362:137104
36. Li ZX, Zhang LM, Udoh II, Ma AL, Zheng YG (2022) Tribol Int 167:107422
37. Zhang L, Qi L, Deng S, Oguntuase O, Deng T, Wang H, Ojo A (2021) Addit Manuf 2021(48):102443
38. Diaz EF, Gonzalez-Rodriguez JG, Martinez-Villafañe A (2010) J Appl Electrochem 2010(40):1633–1640. https://doi.org/10.1007/s10800-010-0149-z
39. Messinese E, Casanova L, Paterlini L, Capelli F, Bolzoni F, Ormellese M, Brenna A (2022) Metals 12:1751. https://doi.org/10.3390/met12101751
40. Vodárek V, Rožnovská G, Kuboň Z, Volodarskaja A, Palupčíková R (2022) Metals 12:1643. https://doi.org/10.3390/met12101643